Journal of Magnetic Resonance 206 (2010) 139–146

Contents lists available at ScienceDirect

Journal of Magnetic Resonance

journal homepage: www.elsevier.com/locate/jmr

Quadrupolar-coupling-specific binomial pulse sequences for *in vivo* ^{23}Na NMR and MRI

Christoffer Laustsen [a,b], Steffen Ringgaard [a], Michael Pedersen [a], Niels Chr. Nielsen [b,*]

[a] MR Research Center, Institute of Clinical Medicine, Aarhus University Hospital, Aarhus, Denmark
[b] Center for Insoluble Protein Structures (inSPIN), Interdisciplinary Nanoscience Center (iNANO), Department of Chemistry, Aarhus University, Aarhus, Denmark

ARTICLE INFO

Article history:
Received 10 April 2010
Revised 24 June 2010
Available online 6 July 2010

Keywords:
Binomial sequences
^{23}Na
Sodium
MRI
NMR
Selective excitation
Quadrupolar coupling specific

ABSTRACT

Aimed at selective detection of ^{23}Na with specific quadrupolar couplings for *in vitro* NMR and MRI, we present a series of quadrupolar binomial pulse sequences offering high specificity with respect to the quadrupolar couplings of the excited species. It is demonstrated that pulse sequences with an increasing number of elements, e.g., 1 1, 1 2 1, 1 3 3 1, 1 4 6 4 1, and 1 5 10 10 5 1, with the units representing flip angles smaller than the 90° pulses typically encountered in binomial spin-1/2 solvent suppression experiments, and different phase combinations may provide a high degree of flexibility with respect to quadrupolar coupling selectivity and robustness towards rf inhomogeneity. This may facilitate efficient separation of, for example, intra and extracellular ^{23}Na in tissues with efficient control of the excitation (or suppression) of central as well as satellite transitions through on- and off-resonance irradiation. The pulse sequences are described in terms of their analogy to binomial liquid-state NMR solvent suppression experiments and demonstrated numerically and experimentally through NMR and MRI experiments on a 7 T horizontal small-bore animal magnet system.

1. Introduction

The sodium gradient plays a pivotal role in cell metabolism and proliferation. ^{23}Na is the second most abundant NMR-active spin species *in vivo*, the spin isotope is 100% abundant, and it is a spin $I = 3/2$ quadrupolar nucleus with a relatively small quadrupole moment, enabling straightforward detection in both liquid and solid phase. In most biological (cellular) environments, ^{23}Na displays non-vanishing quadrupolar interactions with effective quadrupolar coupling constants in the order of 20–550 Hz [1,2] facilitating distinction between intracellular and extracellular sodium compartments in *in vivo* applications. Early studies indicated that the intracellular sodium ions were orientationally constrained leading to isotropic motion without motional narrowing, but with a dominant quadrupolar interaction [2]. The resulting non-vanishing quadrupolar interaction was observed in terms of line broadening through biexponential relaxation with unresolved residual quadrupolar splitting, while later studies reported direct observation of distinct quadrupolar splittings *ex vivo*. Such residual quadrupolar splittings of sodium ions have been reported in human and animal tissues, including, muscle, brain, cartilage, and blood [3].

The existence of ^{23}Na ions with different quadrupolar couplings may be of great interest for several applications. Direct excitation or multiple-quantum filtering facilitates distinction of signals in terms of their quadrupolar couplings [4–7]. Ischemic stroke is an interesting example, where metabolism is disturbed secondary to changes in the Na^+, K^+-ATPase, resulting in increasing intracellular sodium content. The intracellular contribution to the overall ^{23}Na signal is often very small compared to the signal originating from the extracellular space. To address such problems, Lee et al. recently introduced the so-called quadrupolar jump-and-return (QJR) method [6,8], where ^{23}Na spins were excited in a quadrupolar-coupling-specific manner using a pulse sequence bearing resemblance to standard liquid-state NMR binomial solvent suppressions techniques [9–12]. This method was developed numerically using optimal control procedures [13,14] and exploits the different dependencies of the central and satellite transition excitation to rf pulses in a α_{-y}–τ–α_y pulse scheme with the delay adjusted to $\tau = (2n-1)/(2f_Q)$ (using $f_Q = 3\omega_Q/(2\pi)$ with $\omega_Q = 2\pi C_Q/(2I(2I-1))$ denoting the quadrupolar splitting, and n being an integer). A pulse sequence with the pulse flip angle adjusted to $\alpha = 54.7°$ (i.e., the magic angle) facilitates suppression of the satellite transitions while enhancing the amplitude of the central transition relative to normal 90° excitation for the selected quadrupolar coupling. In this study, we take advantage of the analogy between such quadrupolar-coupling-specific pulses and binomial pulse sequences used for water suppression in liquid-state NMR and introduce a series of more advanced binomial pulse sequences, offering a high degree of flexibility in the discriminative excitation of ^{23}Na spins with small

* Corresponding author. Fax: +45 8 6196199.
E-mail address: ncn@inano.dk (N.Chr. Nielsen).

1090-7807/$ - see front matter © 2010 Elsevier Inc. All rights reserved.
doi:10.1016/j.jmr.2010.06.017

differences in the effective quadrupolar coupling constants. As an important additional benefit, some of the pulse sequences are significantly more robust towards experimental artifacts, such as rf inhomogeneity.

2. Theory

The quadrupolar coupling interaction can, in a first-order average Hamiltonian approximation, be described by

$$H_Q^{(1)} = \frac{\omega_Q}{3}[3I_z^2 - I(I+1)] \tag{1}$$

where ω_Q is the quadrupolar coupling frequency (in angular units, *vide supra*), and the operators I_x, I_y, and I_z are the Cartesian angular momentum operators. For a spin $I = 3/2$ nucleus, this Hamiltonian perturbs the $(\pm 3/2, \pm 1/2)$ satellite transitions while it leaves the $(1/2, -1/2)$ central transition unaffected. This effect can be exploited to discriminate spins with different quadrupolar coupling interactions. In the present study, we examined a set of binomial pulse sequences of the type 1 1, 1 2 1, 1 4 6 4 1, 1 3 3 1, and 1 5 10 10 5 1, as well as their phase-inverted variants $1\bar{1}$, $1\bar{2}1$, $1\bar{3}3\bar{1}$, $1\bar{4}6\bar{4}1$, and $1\bar{5}10\overline{10}5\bar{1}$. A bar over a pulse indicates negative rf phase. Each pair of numbers represents pulses separated by a delay τ, e.g., $1\bar{2}1$ denotes a $(\alpha)_x - \tau - (2\alpha)_{-x} - \tau - (\alpha)_x$ sequence, where the sum 4α of unit flip angles (α) typically is adjusted to 90° for liquid-state NMR solvent suppression. The delay is adjusted to $\tau = 1/(2n\Delta\nu^{\max})$ with the carrier being on the resonance with respect to the spin to observe and the distance from the carrier to the resonance to be suppressed being $\Delta\nu^{\max}$ (n being an integer). We note that it is beyond the scope of the paper to address specifically the effects of relaxation, implying that potential strong effects from relaxation should be considered in the choice of the optimal experiment.

The idea behind the quadrupolar variants of binomial pulse sequences is similar to the solvent-suppression methods in the sense that sequences with appropriate pulse flip angles and delays relative to the distinct quadrupolar coupling frequency of a specific ingredient may offer flexibility to enhance or suppress excitation of certain transitions for spins with a specific quadrupolar coupling. It is clear that an on-resonance antiphase pulse sequence will in absence of quadrupolar coupling (assuming infinitely strong, short pulses) leave the spins invariant, while the presence of a finite quadrupolar coupling may cause dephasing of the signal in-between the pulses, leading to perturbation that depends on C_Q. Here we extend the analysis of quadrupolar analogs to liquid-state NMR solvent-suppression methods to more advanced binomial sequences motivated by the fact that sequences such as 1 3 3 1 have proven significantly better than the simple 1 1 jump-and-return sequence in the spin-1/2 case [8,15].

2.1. Analytical description of bionomial sequences

On basis of the quadrupolar coupling Hamiltonian and relevant initial and desired final spin states (e.g., using *Mathematica* [16] – see Supplementary Material for examples), it is relatively easy to derive expressions for the transfer of polarization (I_z) into −1-quantum coherence (I^-) on the central $(1/2, -1/2)$ transition (Intensity: $\langle I_{cen}^- \rangle$) and each of the satellite transitions $(\pm 3/2, \pm 1/2)$ transitions (Intensity (each transition): $\langle I_{sat}^- \rangle$). Such expressions may provide an overview of the potential of increasingly complex binomial sequences, although restrictions in the parameter space have to be taken to get meaningful expressions for the most advanced sequences. Our analysis was confined to pulse sequences using $\theta = \omega_Q\tau = n\pi/3$ with $n = 0, 1$, $\omega_Q = \pi C_Q/3$, and $\tau = 1/C_Q$ – a more extended analysis (not shown) did not provide better solutions.

For the 1 1 and $1\bar{1}$ sequences, we obtain:

$$\begin{aligned}
\langle I_{cen}^- \rangle(1\,1)^{\pi/3} &= \frac{1}{80}(2s_{2\alpha} - 9s_{4\alpha}) \\
\langle I_{sat}^- \rangle(1\,1)^{\pi/3} &= -\frac{9}{10}c_\alpha s_\alpha^3 \\
\langle I_{cen}^- \rangle(1\,1)^{0} &= -\frac{2}{10}s_{2\alpha} \\
\langle I_{sat}^- \rangle(1\,1)^{0} &= -\frac{3}{10}s_{2\alpha}
\end{aligned} \tag{2}$$

$$\begin{aligned}
\langle I_{cen}^- \rangle(1\,\bar{1})^{\pi/3} &= \frac{9}{10}s_\alpha^3 c_\alpha \\
\langle I_{sat}^- \rangle(1\,\bar{1})^{\pi/3} &= \frac{3}{10}s_\alpha c_\alpha(3c_\alpha^2 - 1) \\
\langle I_{cen}^- \rangle(1\,\bar{1})^{0} &= \langle I_s^- \rangle(1\,\bar{1})^{0} = 0
\end{aligned} \tag{3}$$

where the value of q is given as superscript and we introduced the short-hand notations: $c_x = \cos(x)$ and $s_x = \sin(x)$. It is evident that the 1 1 sequence with $\theta = 0°$ does not allow for discrimination of different transitions, but may be used to excite both operators simultaneously using $\alpha = 45°$ leading to maximal efficiencies of 0.2 and 0.3 for the central and satellite transitions, respectively. The 1 1 sequence with $\theta = \pi/3$ and $\alpha = 41.81°$ suppresses the central transition while exciting each satellite transition with an efficiency of 0.20. Using $\theta = \pi/3$ and $\alpha = 15.37°$, the central transition is excited with an efficiency of 0.09, while the satellite transitions are suppressed to 0.02.

The $1\bar{1}$ antiphase experiment using $\theta = \pi/3$ and $\alpha = 54.7°$, as described previously by Lee et al. [8], suppresses the satellite transitions while exciting the central transition with an efficiency of 0.28 representing an enhancement of 41% relative to the single-pulse 90° experiment. Using $\alpha = 18.6°$, the satellite transitions may be excited with efficiency of 0.16 while the central transition is attenuated to 0.03.

For the three-element 1 2 1 and $1\bar{2}1$ sequences, we obtain

$$\begin{aligned}
\langle I_{cen}^- \rangle(1\,2\,1)^{\pi/3} &= -\frac{1}{160}(-3 + 32c_{2\alpha} + 18c_{4\alpha} + 9c_{6\alpha} + 9c_{8\alpha})s_{2\alpha} \\
\langle I_{sat}^- \rangle(1\,2\,1)^{\pi/3} &= \frac{3}{40}(5c_\alpha + 6c_{3\alpha} - 3c_{7\alpha})s_\alpha^3 \\
\langle I_{cen}^- \rangle(1\,2\,1)^{0} &= -\frac{2}{10}s_{4\alpha} \\
\langle I_{sat}^- \rangle(1\,2\,1)^{0} &= -\frac{3}{10}s_{4\alpha}
\end{aligned} \tag{4}$$

$$\begin{aligned}
\langle I_{cen}^- \rangle(1\,\bar{2}\,1)^{\pi/3} &= \frac{3}{20}c_\alpha(1 + 3c_{4\alpha})s_\alpha^3 \\
\langle I_{sat}^- \rangle(1\,\bar{2}\,1)^{\pi/3} &= -\frac{3}{80}(1 + 3c_{2\alpha})(1 + 3c_{4\alpha})s_{2\alpha} \\
\langle I_{cen}^- \rangle(1\,\bar{2}\,1)^{0} &= \langle I_s^- \rangle(1\,\bar{2}\,1)^{0} = 0
\end{aligned} \tag{5}$$

The inphase 1 2 1 sequence with $\theta = 0°$ and $\alpha = 22.5°$ excites the central and satellite transitions, resulting in maximum efficiencies of 0.20 and 0.30 for, respectively. Using $\theta = \pi/3$, the satellite transitions are suppressed for $\alpha = 40.5°$ leading to an efficiency of 0.08 for the central transition.

By differentiating the central transition intensity expression for the antiphase $1\bar{2}1$ pulse sequence with $\theta = \pi/3$ with respect to α, we find an extremum point at $\alpha = 48.5°$ leading to an efficiency of 0.08 for the central transition while each satellite transition is attenuated to 0.01. Full suppression of the satellite transitions may be obtained for $\alpha = 54.7°$, leading to an efficiency of 0.06 for the central transition. The $1\bar{2}1$ sequence with $\theta = \pi/3$ displays maximum difference in the excitation efficiencies for the satellite and central transitions for $\alpha = 13.41°$, in which case efficiencies of 0.18 and 0.01 are obtained, respectively.

For the four-element 1 3 3 1 and $1\bar{3}3\bar{1}$ pulse sequences, we obtain

$$\begin{aligned}
\langle I^-_{cen}\rangle(1331)^{\pi/3} &= -\frac{1}{640}(132-104c_{2\alpha}+189c_{4\alpha}-65c_{6\alpha}+162c_{8\alpha}\\
&\quad +72c_{10\alpha}+36c_{12\alpha}+72c_{14\alpha}+9c_{18\alpha}+9c_{20\alpha})s_{2\alpha}\\
\langle I^-_{sat}\rangle(1331)^{\pi/3} &= \frac{9}{80}c_\alpha(7+26c_{2\alpha}+14c_{4\alpha}+13c_{6\alpha}+c_{8\alpha}+3c_{10\alpha}\\
&\quad -3c_{12\alpha}+3c_{14\alpha}+c_{16\alpha}-c_{18\alpha})s^3_\alpha\\
\langle I^-_{cen}\rangle(1331)^{0} &= -\frac{2}{10}s_{8\alpha}\\
\langle I^-_{sat}\rangle(1331)^{0} &= -\frac{3}{10}s_{8\alpha}
\end{aligned} \tag{6}$$

$$\begin{aligned}
\langle I^-_{cen}\rangle(1\bar{3}3\bar{1})^{\pi/3} &= \frac{9}{40}c_\alpha(-3-4c_{2\alpha}+3c_{6\alpha})(1+4c_{2\alpha}+3c_{6\alpha})s^3_\alpha\\
\langle I^-_{sat}\rangle(1\bar{3}3\bar{1})^{\pi/3} &= \frac{3}{1280}(16s_{2\alpha}-22s_{4\alpha}-3s_{8\alpha}+42s_{10\alpha}\\
&\quad +18s_{14\alpha}+27s_{16\alpha})\\
\langle I^-_{cen}\rangle(1\bar{3}3\bar{1})^{0} &= \langle I^-_{s}\rangle(1\bar{3}3\bar{1})^{0} = 0
\end{aligned} \tag{7}$$

The 1 3 3 1 sequence with $\theta = 0°$ and $\alpha = 11.3°$ leads to the maximum efficiencies of 0.20 and 0.30, for the central and satellite transitions, respectively. The satellite transitions may be excited with efficiency of 0.10, while the central transition is suppressed, using $\theta = \pi/3$ and $\alpha = 69.0°$. For the $1\bar{3}3\bar{1}$ sequence with $\theta = \pi/3$ and $\alpha = 58.6°$ one obtains central and satellite transition efficiencies of 0.28 and 0, respectively, while the sequence with $\alpha = 7.1°$ excites the central and satellite transitions with efficiencies of 0.02 and 0.17, respectively.

On basis of this analysis, we conclude that the inphase sequences with $\theta = 0°$ generally leads to good solutions for simultaneous excitation of both central and satellite transitions with maximal efficiencies of 0.2 and 0.3, respectively. The antiphase sequences, however, offer better possibilities to distinguish these signal components, with the $1\bar{1}$ and $1\bar{3}3\bar{1}$ sequences with $\theta = \pi/3$ allowing for selective excitation of the central and satellite transitions with efficiencies of 0.28 and 0.17, respectively.

2.2. Numerical analysis of binomial sequences

Aimed at obtaining more detailed insight into the various binomial sequences with respect to quadrupolar coupling selectivity and robustness towards, e.g., rf inhomogeneity, we, inspired by the analytical solutions, expanded our analysis with numerical simulations. These were performed using the open-source NMR simulation software SIMPSON [13]. Two separate analyses were performed. (1) Providing an "unfiltered" picture of the efficiency of transfer into the central and satellite transitions as functions of θ and α, giving full flexibility to find sequences with any combination of transfers into these transitions. (2) Simulations of a more conditional nature, where the corresponding plots are "filtered" to present solutions only which excites the desired type of transitions above a certain threshold (set to ±20% of the maximum intensity)

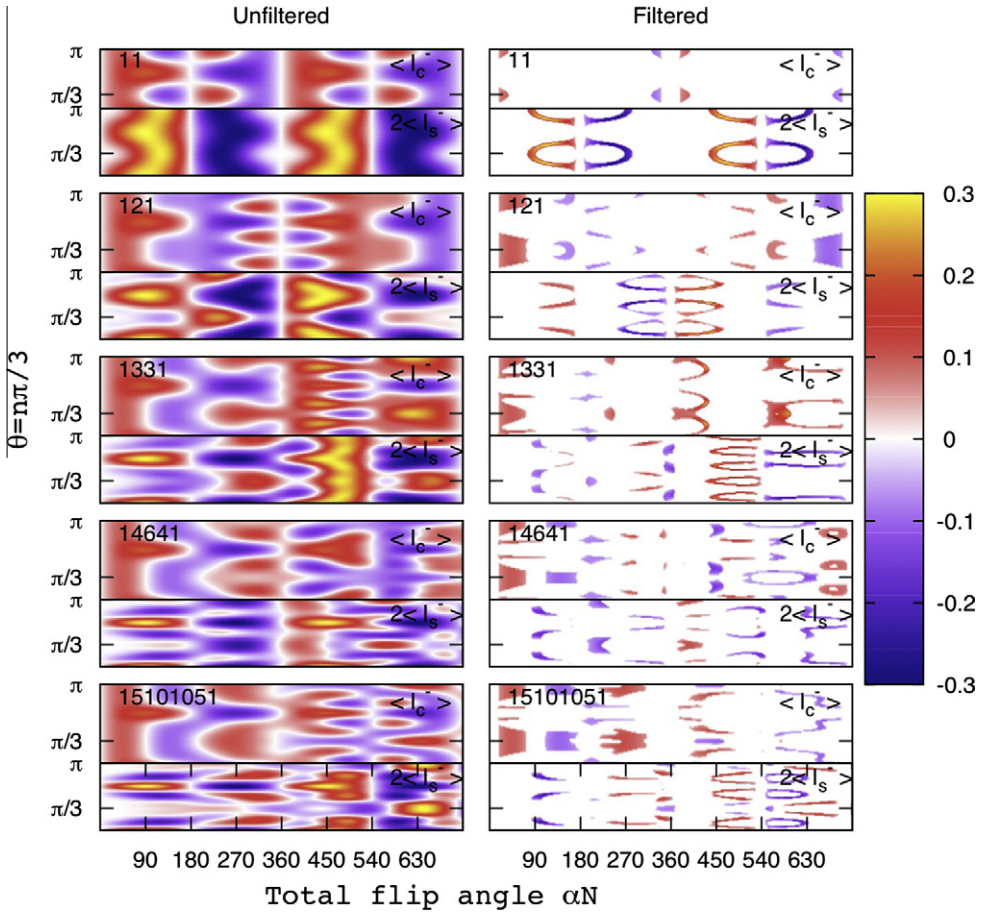

Fig. 1. ^{23}Na 2D excitation profiles for the central ($\langle I^-_{cen}\rangle$; upper panels) and satellite ($2\langle I^-_{sat}\rangle$; sum for the two transitions; lower panels) transitions as function of the total flip angle $N\alpha$ and the quadrupolar evolution angle θ for various inphase quadrupolar bionomical sequences. (left row) Unfiltered signal intensities. (right row) Filtered signal intensities confined to regions, where the desired transition is excited above ±20% of the maximal intensity, while the nondesired transition is suppressed to be in the range ±10% of its maximal intensity. The colorcode reflects efficiencies ranging from −0.3 to 0.3 in consistency with the analytical description (see text).

while suppressing the undesired type below a certain threshold (set to ±10% of the maximum intensity). This provides easier access to typical pulse sequences for practical filtering applications. To facilitate easy accessible comparison of sequences with different number of elements, we scaled the dependency on the pulse flip angle α by total number of pulse units N (i.e., $N = 2$ for 1 1, $N = 4$ for 1 2 1, etc.), leading to a unified dependency on the angle αN in our analysis.

Fig. 1 shows unfiltered and filtered intensity plots for the central and satellite transitions excited using inphase binomial sequences. The plots clearly reveal a cyclic dependency on the pulse flip angles α and the delay τ, matched to the quadrupolar coupling through the angle θ. We note that the latter relation allows these plots to be used to predict the performance of pulse sequence for any desired quadrupolar coupling frequency. It is evident from the unfiltered plots that the intensity extrema for the central and satellite transitions often occurs for the same values of θ and α and that the cyclic dependency on θ leads to good excitations for both type of transitions at $\theta = n\pi/3$, where n is an even integer. At these points, the extremum efficiencies for the central and satellite transitions may reach 0.20 and 0.30, respectively, as predicted analytically. These solutions provide good overall MRI sensitivity in cases, where the combined response from central and satellite transitions (adding the sensitivity for the central transition and the two satellite transitions) are desired for specific values of C_Q. For *in vivo* applications, it may be advantageous to use higher-order binomial pulses, as the "broad C_Q distribution" solutions of the 1 1 pulse may cause unwanted signals from undesired constituents characterized by a different quadrupolar coupling. Moving the transmitter to one of the satellites, as an example, enables the excitation of that given quadrupolar coupling, while suppressing constituents with $C_Q = 0$. Less efficiency is generally obtained for odd values n, which is unfortunate in the sense that the filtered plots reveal that the most discriminating solutions are found in this case. The best solutions include selective excitation of the satellite transitions in archs around $\theta = \pi/3$ and $\alpha > \pi/2$ for the 1 1 sequence, while selective excitation of the central transition is obtained for much smaller values of α.

Fig. 2 shows the corresponding unfiltered and filtered intensity plot for the phase-alternated binomial pulse sequences, These plots reveal a markedly different distribution of intensity between the central and satellite transitions, enabling much easier and more efficient discrimination of these transitions as particularly evident from the filtered plots. This applies in particular to sequences with an even number of elements like $1\bar{1}$ and $1\bar{3}3\bar{1}$, which we may accordingly recommend in favour of odd-element sequences like $1\bar{2}1$ and $1\bar{4}6\bar{4}1$ typically providing less efficient excitation of all transitions. The plots also reinforce our earlier observation that sequences with more elements have better conditions with respect to sharp filtering of signals due to their quadrupolar coupling (narrower solutions along the vertical axis) *and* at the same time much more robustness towards variations in the pulse flip angles αN (broader solutions along the horizontal axis), as may be induced by inhomogeneous rf fields.

Fig. 3 shows expanded views of the filtered intensity plots for the $1\bar{1}$ and $1\bar{3}3\bar{1}$ sequences with τ values of $1/C_Q$ and $1/(3C_Q)$. It

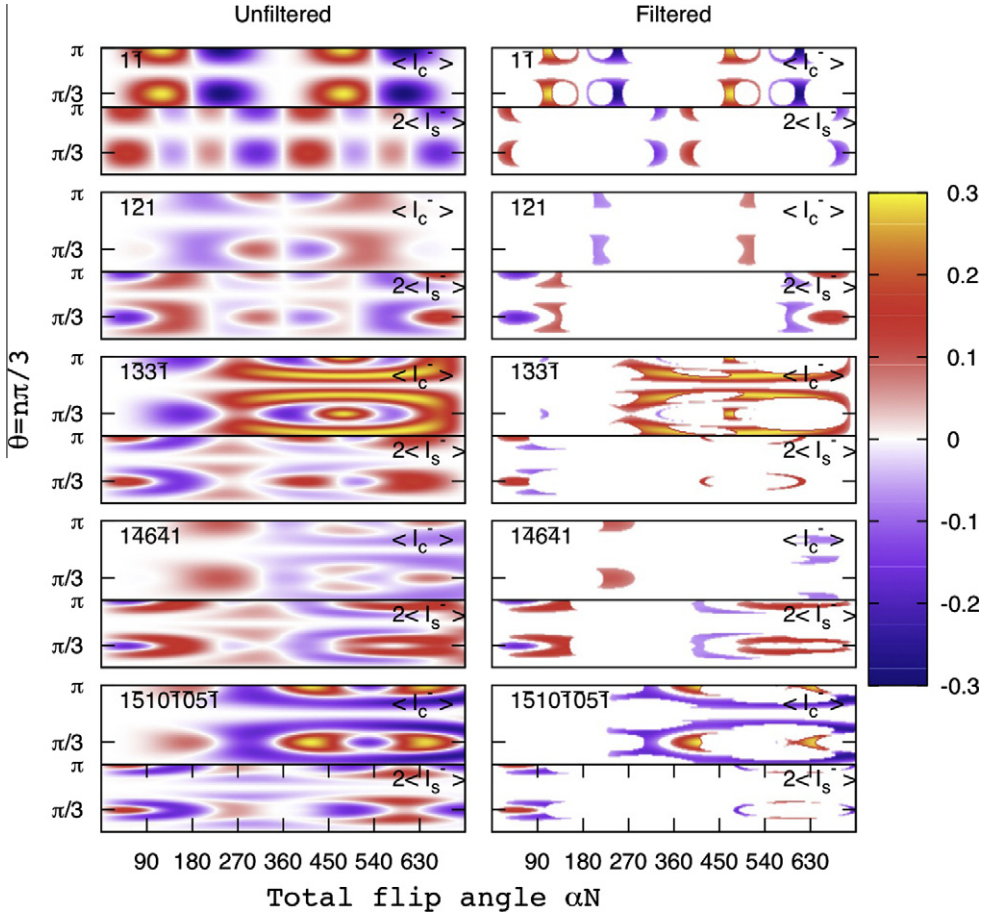

Fig. 2. ^{23}Na 2D excitation profiles for the central ($\langle I^-_{cen}\rangle$; upper panel) and satellite ($2\langle I^-_{sat}\rangle$; sum for the two transitions; lower panel) transitions as function of the total flip angle $N\alpha$ and the quadrupolar evolution angle θ for various antiphase quadrupolar bionomical sequences. (left row) Unfiltered signal intensities, (right row) filtered signal intensities confined to regions as described for Fig. 1. The colorcode reflects efficiencies ranging from −0.3 to 0.3 in consistency with the analytical description (see text).

is evident that the satellite transitions are suppressed completely for the $1\bar{1}$ sequence with $\alpha = 109.4°/2 = 54.7°$ and the $1\bar{3}3\bar{1}$ sequence with $\alpha = 469°/8 = 58.6°$ in both cases using $\tau = 1/C_Q$ (marked by crosses in Fig. 3), in agreement with our analytical findings. We note that full suppression of the satellites for the $1\bar{3}3\bar{1}$ sequence is obtained at the expense of a slight reduction of the central transition amplitude having its maximum at $\alpha = 495.2°/8 = 61.9°$. The expanded regions for the $1\bar{3}3\bar{1}$ sequences with τ equal to $1/C_Q$ and $1/3C_Q$ in Fig. 3 reveal clearly the diversity in the solutions in terms of three practically important issues, namely the quadrupolar-coupling-specificity/broadbandedness, the robustness towards rf inhomogeneity or mismatch, and the overall length of the sequence.

Addressing the first point, it is clear that $1\bar{3}3\bar{1}$ sequences with τ equal to $1/C_Q$ or $1/(3C_Q)$ may be tuned to be highly specific with respect to C_Q (narrow excitation bands in the vertical dimension) or conversely be robust to variations in C_Q (broad excitation bands in the vertical dimension). It is also clear that these sequences may be extremely broadbanded with respect to variations in α and thereby towards rf inhomogeneity or flip angle maladjustments (i.e., broad excitation bands in the horizontal dimension). By increasing the complexity of the pulse sequence, the number of interpulse delay units is increased, which intuitively may lead to an unacceptable lengthening of the experiment thereby reducing the potential for higher-order sequences in *in vivo* applications due to relaxation. By inspection of the contour plots in Figs. 1 and 3, however, one readily finds good $1\bar{3}3\bar{1}$ binomial sequences with $\theta = n\pi/9$, n being an odd integer that reduces the pulse sequence length by a factor of $3k$ using $\tau = 1/(3kC_Q)$ with k being an integer. In this manner, it is possible to significantly diminish the losses due to relaxation and at the same time improve the robustness toward rf inhomogeneity significantly through an extended α range. We note, however, that this reduction comes at the expense of a broader C_Q range for the excitation, and thereby reduced quadrupolar-coupling-specific site discrimination as illustrated in Fig. 3D, also containing the corresponding curve for the $1\bar{1}$ binomial sequence with $\tau = 1/C_Q$. It is clearly evident that the C_Q discrimination capability of the equally long $1\bar{1}$ with $\tau = 1/C_Q$ and $1\bar{3}3\bar{1}$ with $\tau = 1/(3C_Q)$ sequences is similar, however, with a markedly improved rf variation robustness of the latter sequence.

The presence of efficient $1\bar{3}3\bar{1}$ experiments with $\theta = \pi/9$ may readily be confirmed by the analytical formula

$$\begin{aligned}\langle I^-_{cen}\rangle(1\bar{3}3\bar{1})^{\pi/9} &= \frac{9}{2560}c_\alpha(-16c_{2\alpha}+3(-9+c_{6\alpha}))\\ &\quad(-11+16c_{2\alpha}+3c_{6\alpha})s_\alpha^3\\ \langle I^-_{sat}\rangle(1\bar{3}3\bar{1})^{\pi/9} &= \frac{3}{81920}(-104s_{2\alpha}+362s_{4\alpha}\\ &\quad-867s_{8\alpha}-318s_{10\alpha}+18s_{14\alpha}+27s_{16\alpha})\end{aligned} \tag{8}$$

revealing optimal attenuation of the satellite transitions for $\alpha = 70.3°$ with the central transition excited with an efficiency of 0.29. By plotting the central transition efficiency (Fig. 3B), we find that a broader range for the θ angle may be obtained by reducing the interpulse delay slightly more.

3. Experimental

All NMR and MRI experiments were carried out on a 7 T horizontal 11 cm bore magnet (Oxford Instruments, Oxford, United Kingdom) equipped with a Varian Unity Inova console (Varian Inc, Palo Alto, CA, USA) and a gradient system for imaging (Tesla Engineering, West Sussex, United Kingdom). The acquisition software was Vnmr 6.1c and Vnmrj 1.0.6c (Varian, Paolo Alto, CA, USA). Spectroscopy experiments were conducted using a standard gradient echo sequence with the excitation pulse substituted by a

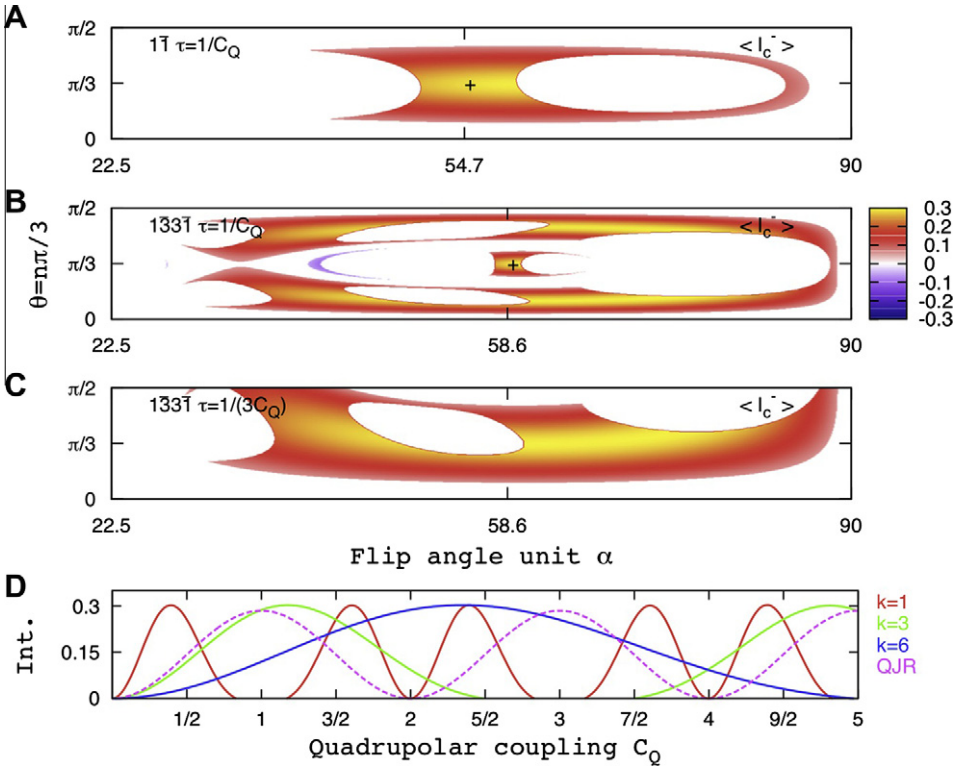

Fig. 3. Expansions of 2D central transition filtered excitation plots (from Fig. 2; filtering as described in Fig. 1) for the (A) $1\bar{1}$ ($\tau = 1/C_Q$), (B) $1\bar{3}3\bar{1}$ ($\tau = 1/C_Q$), and (C) $1\bar{3}3\bar{1}$ ($\tau = 1/(3C_Q)$) binomial pulse sequences. The analytical results are marked in each of the two with (+). (D) Central transition excitation efficiencies for $1\bar{3}3\bar{1}$ binomial pulse sequences with $\tau = 1/(3kC_Q)$, $k = 1$, 2, and 3, as function of C_Q. The dashed line corresponds to data obtained with the $1\bar{1}$ QJR sequence with $\tau = 1/C_Q$. The colorcode reflects efficiencies ranging from −0.3 to 0.3 in consistency with the analytical description (see text).

non-selective square-shape pulse or a binomial pulse. Imaging experiments were performed with a short constant echo time to ensure as high signal as possible from fast relaxing sodium ions. A concern when moving up through the binomial series is the increasing evolution time, which may cause considerable signal loss due to spin relaxation and potentially inhomogeneity. This can be partly overcome by inserting refocusing pulses in-between the pulse segments, creating a binomial excitation that is T_2- rather than T_2^*-dependent [8], or by reducing the interpulse delays (*vide supra*). In this regard we note that central (T2s) and satellite (T2f) transition transverse relaxation rates in the ranges of 20–24 ms and 3.5–5 ms, respectively, has been reported for porcine skeletal muscle and cat brain [17]. Albeit the gradient echo sequence used in this study can be used with shorter echo times, UTE sequences like the SPRITE sequence [18], may be preferable for *in vivo* imaging influenced significantly by relaxation.

Experiments were carried out on Pf1 bacteriophage (ASLA Biotech, Riga, Latvia) and a linoleic acid sodium salt (Sigma) to induce a finite quadrupolar splitting for ^{23}Na in solution. Using a standard PBS buffer and Pf1 at a concentration of 30 mg/ml, the sodium ions displayed a quadrupolar splitting of $f_Q = 275$ Hz, corresponding to $C_Q = 550$ Hz.

Data processing was performed using iNMR 2.6.2 (Nucleomatica, Molfetta, Italy) and Matlab (MathWorks, Inc., Natick, USA). MR images were viewed and analysed using the ImageJ software (rsbweb.nih.gov), [19]. Numerical simulations were carried out using the open-source software package SIMPSON [13], while analytical density matrix calculations, where performed using *Mathematica* [16] (Wolfram Research, Inc., Champaign, USA).

4. Results and discussions

The basic $1\bar{1}$ ($\alpha = 54.7°$) and $1\bar{3}3\bar{1}$ ($\alpha = 58.63°$) binomial gradient echo experiments with $\tau = 1/C_Q$ are compared with standard single-pulse excitation (excitation of full sample) in Fig. 4 showing ^{23}Na spectra (upper row), images (middle row), and traces through images obtained for a phantom containing Pf1 bacteriophage ($C_Q = 550$ Hz) in the inner ring, and a saline solution ($C_Q = 0$) in the outer ring (geometry in upper-right corner of Fig. 4). From these plots it is evident that the binomial sequences suppress the satellite transitions, while exciting exclusively the central transition for the quadrupolar coupling of the bacteriophage in the inner ring. The 1D spectra (top) and the traces (bottom) through the images (middle) that are going from the single-pulse, non-discriminative experiments, through the two-element antiphase sequence to the four times longer four-element sequence is associated with a substantial loss in signal-to-noise due to relaxation. We note that the prolonged evolution time is expected to reduce the fast relaxing satellite transition significantly from the Pf1 vial, while the central transition of the two vials relax at equal rates. This may suggest that the $1\bar{3}3\bar{1}$, though reduced in efficiency, has selectivity advantages over the $1\bar{1}$ pulse.

At the expense of less precise discrimination of signals in terms of quadrupolar coupling constants (i.e., enlarged C_Q excitation bandwidth), the sensitivity loss seen for the $1\bar{3}3\bar{1}$ pulse sequence in Fig. 4, may be reduced with the additional benefit of improved robustness towards rf inhomogeneity relative to the $1\bar{1}$ binomial sequence. A three fold and beyond reduction in the length of the four-element sequence may be obtained through adjustment of

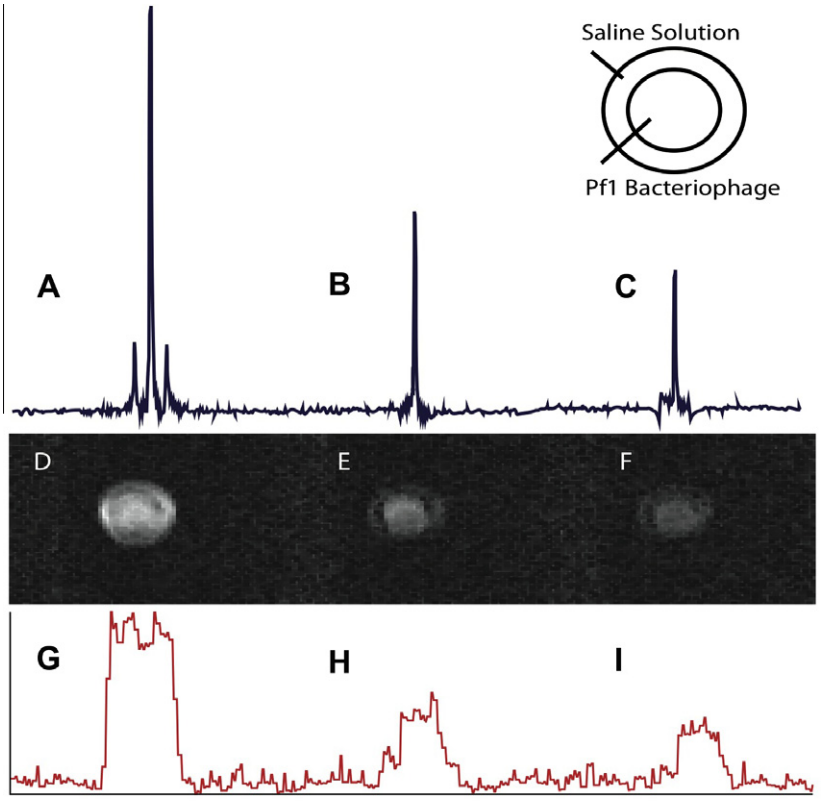

Fig. 4. Experimental comparison of single-pulse, $1\bar{1}$ ($\alpha = 54.7°$, $\tau = 1/C_Q$) binomial, and $1\bar{3}3\bar{1}$ ($\alpha = 58.63°$, $\tau = 1/C_Q$) binomial gradient echo experiments obtained for a phantom containing two concentric vials (schematic drawing in upper-right corner) containing 77 mM Na^+ ions in both vials, with the inner vial containing a 2.7 mL standard PBS solution and 1.6 mL Pf1 solution while the outer vial contains a saline solution. (A–C) ^{23}Na spectra for the full sample volume and (D–F) ^{23}Na gradient echo images (projected slice, non-selective square pulse) obtained using (A, D) 90° single-pulse excitation, (B, E) $1\bar{1}$ ($\alpha = 54.7°$, $\tau = 1/C_Q$) binomial excitation, and (C, F) $1\bar{3}3\bar{1}$ ($\alpha = 58.63°$, $\tau = 1/C_Q$) binomial excitation. (G–I) Trace taken through the images in the row above.

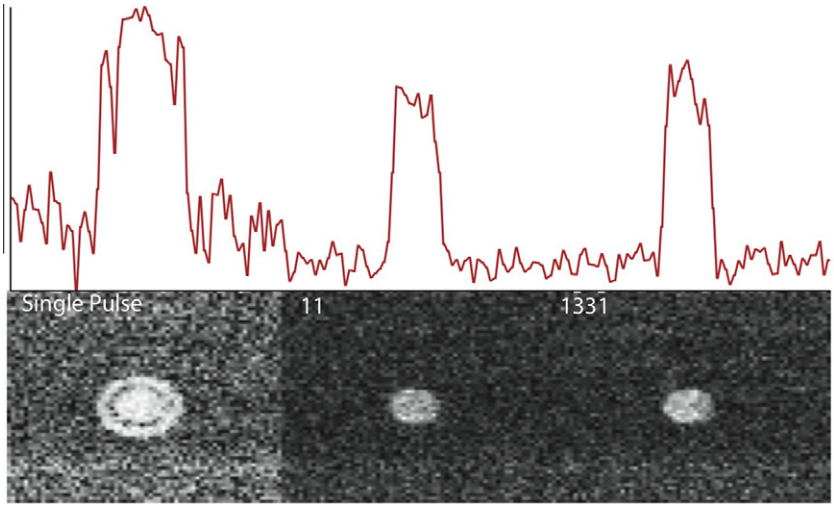

Fig. 5. Experimental ^{23}Na gradient echo coronal images (lower row) and 1D traces through these (upper row) obtained for the phantom described in Fig. 4, using (left) 90° single-pulse excitation, (middle) $1\bar{1}$ ($\alpha = 54.7°$, $\tau = 1/C_Q$) binomial excitation, and (right) $1\bar{3}3\bar{1}$ ($\alpha = 70.25°$, $\tau = 1/(3C_Q)$) binomial excitation. Thirty-two transients were used for the single-pulse excitation, while 128 transients were used for the binomial excitations. For all three experiments we used TR = 300, TE = 4.32 ms, coronal projection with a resolution of 0.9375 × 0.9375 mm.

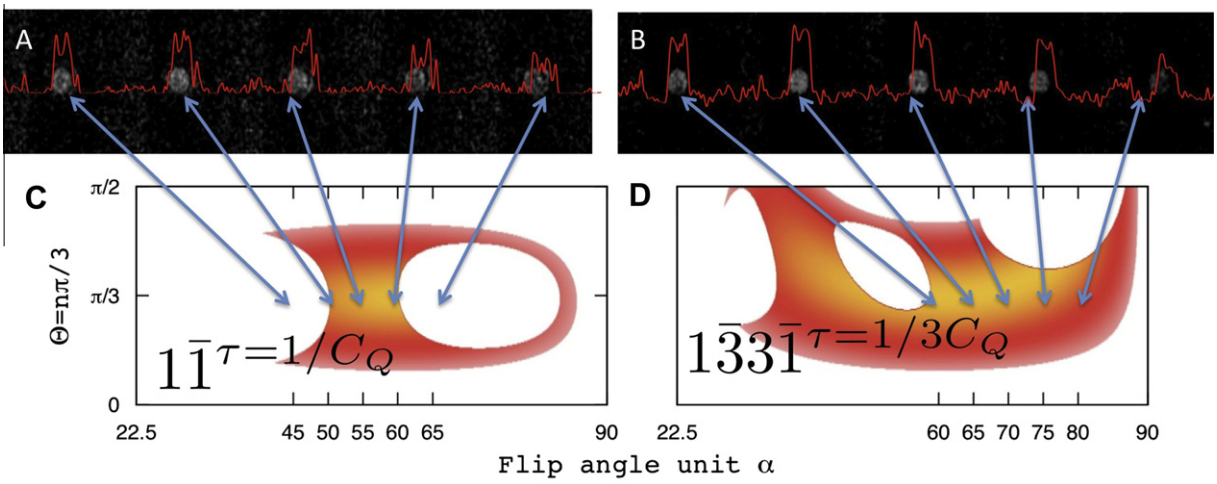

Fig. 6. A. Series of five experimental ^{23}Na gradient echo coronal images obtained using $1\bar{1}$ ($\alpha = 45–65°$, $\tau = 1/C_Q$) excitation and the corresponding 1D traces through these for the phantom described in Fig. 4B. Series of five experimental ^{23}Na gradient echo coronal images obtained using $1\bar{3}3\bar{1}$ ($\alpha = 60–80°$, $\tau = 1/(3C_Q)$) excitation and corresponding 1D traces. The binomial excitation sequences used pulse flip angles varied over a span of 20° around the nominal flip angle (55° for $1\bar{1}$ and 70° for $1\bar{3}3\bar{1}$) to explore the effect of rf field strength variation C and D. 2D excitation plots showing the efficiency of the binomial excitation as a function of the angle α and the quadrupolar evolution angle θ with the contour plot from Fig. 2 inserted to correlate the experimental observations with numerical data. Both experiments used TR/TE = 300/4.32 ms, a matrix of 64 × 64, FOV 6 × 6 cm. The intensities correspond to the color bar in Figs. 1–3. (For interpretation of the references to color in this figure legend, the reader is referred to the web version of this article.)

the sequence to $\theta = \pi/9$ centred around the C_Q value of interest. Fig. 5A compares images for the same phantom as used for Fig. 4 obtained using single 90° pulse excitation, $1\bar{1}$ with $\tau = 1/C_Q$, and $1\bar{3}3\bar{1}$ with $\tau = 1/(3C_Q)$ (i.e., $\theta = \pi/9$). In this case the two latter images (as seen through the traces shown below the images) are similar in intensity, potentially with a smoother profile for the $1\bar{3}3\bar{1}$ image than for the $1\bar{1}$ image potentially due to improved rf inhomogeneity compensation.

The markedly improved robustness towards rf inhomogeneity/variations for the $1\bar{3}3\bar{1}$ ($\tau = 1/(3C_Q)$; $\theta = \pi/9$; $\alpha = 70°$) sequence relative to the equally long $1\bar{1}$ ($\tau = 1/C_Q$; $\theta = \pi/3$; $\alpha = 54.7°$) sequence is illustrated in Fig. 6 by images of the bacteriophage/saline phantom along with traces through the images and the corresponding α/θ plots. For both sequences experimental images were generated as function of the total flip angle $N\alpha$ arrayed over 20° around the optimal value, corresponding to the points marked with arrows in the 2D α/θ excitation plots (taken from Fig. 3). It is evident that the $1\bar{3}3\bar{1}$ $\theta = \pi/9$ bionomial sequence is superior to the $1\bar{1}$ $\theta = \pi/3$ bionomial sequence with respect to both overall efficiency and robustness towards rf field variations. It is also found that the $1\bar{3}3\bar{1}$ do not excite signals from the outer ($C_Q = 0$) vial, while the $1\bar{1}$ does that to a minor extend. We should also note that contrast signal-to-noise ratio (CNR) is higher for the $1\bar{3}3\bar{1}$ sequence and the excitation is more uniform across the inner vial, than for the $1\bar{1}$ sequence.

The results presented above concern exclusively discrimination of components with different quadrupolar couplings through excitation of the central transition. As evident from Fig. 2, all antiphase binomial pulse sequences may be used for excitation of the satellite transitions instead, using solutions with $N\alpha < 90°$. However, these sequences lack signal amplitude relative to the $N\alpha > 90°$ counterparts mediating transfer through the central transition.

Addressing attention to the inphase variants, they may beneficially be used for relaxation studies, where only the single exponential decay is present or for reducing image blurring caused by the satellites transition. By increasing the total flip angle $N\alpha > 90^\circ$ for the inphase variants, we may obtain the same effects as for the antiphase variants, however, with lower efficiency. Finally, we note that higher-order sequences (inphase as well as antiphase) generally provide increased selectivity towards C_Q and that great flexibility exists with respect to choosing sequences fulfilling specific needs, on basis of the analysis provided in the preceding section. The sequence of choice should be chosen under consideration of the quadrupolar coupling (typical values of 20–600 Hz *in vivo*) and relaxation parameters for a given application.

5. Conclusions

In conclusion, we have demonstrated that higher-order binomial pulse sequences, as originally known for water suppression in spin $I = 1/2$ liquid-state NMR spectroscopy, offer interesting perspectives for studies of ^{23}Na in *in vivo* applications. Relative to the previous $1\,\bar{1}$ pulse sequence, higher-order inphase and in particular antiphase pulse sequences may provide substantially improved specificity towards C_Q (or conversely increased bandwidth, if desired) and improved robustness towards rf inhomogeneity. We have presented an analytical and numerical analysis of the various pulse sequences, and have provided a graphical representation allowing for selection of pulse sequences to use for quadrupolar-specific excitation in practical applications. While our first presentation of the quadrupolar bionomial pulse sequences addressed *in vitro* phantoms, we expect that the pulse sequences will find widespread application in *in vivo* ^{23}Na MRI and MRS. Such experiments will take advantages of the distinct ^{23}Na quadrupolar coupling parameters known to exist in cellular/organ systems. We are currently exploring such applications in animal models.

Acknowledgments

We acknowledge support from the Danish National Research Foundation and the Danish Center for Scientific Computing. The authors would like to acknowledge Gitte Kall for creating the NMR samples.

Appendix A. Supplementary material

Supplementary data associated with this article can be found, in the online version, at doi:10.1016/j.jmr.2010.06.017.

References

[1] C. Hughes, R. Kemp-Harper, P. Styles, S. Wimperis, N.M.R. Spectroscopy, NMR spectroscopy and imaging of sodium in ordered environments. The return of the central transition, J. Magn. Reson. B. 111 (1996) 189–193.
[2] A. Borthakur, E. Mellon, S. Niyogi, W. Witschey, Sodium and T1 MRI for molecular and diagnostic imaging of articular cartilage, NMR Biomed. 19 (2006) 781–821.
[3] H. Shinar, T. Knubovets, U. Eliav, G. Navon, Sodium interaction with ordered structures in mammalian red blood cells detected by Na-23 double quantum NMR, Biophys. J. 64 (1993) 1273–1282.
[4] K. Ooms, M. Cannella, A. Vega, M. Marcolongo, 23Na TQF NMR imaging for the study of spinal disc tissue, J. Magn. Reson. 195 (2008) 112–115.
[5] J. Choy, W. Ling, A. Jerschow, Selective detection of ordered sodium signals via the central transition, J. Magn. Reson. 180 (2006) 105–109.
[6] J.-S. Lee, R.R. Regatte, A. Jerschow, Optimal nuclear magnetic resonance excitation schemes for the central transition of a spin 3/2 in the presence of residual quadrupolar coupling, J. Chem. Phys. 129 (2008) 4510–4516.
[7] J.-S. Lee, R.R. Regatte, A. Jerschow, Optimal excitation of 23Na nuclear spins in the presence of residual quadrupolar coupling and quadrupolar relaxation, J. Chem. Phys. 131 (2009) 4501–4509.
[8] J. Lee, R. Regatte, A. Jerschow, Selective detection of ordered sodium signals by a jump-and-return pulse sequence, J. Magn. Reson. 200 (2009) 126–129.
[9] P.J. Hore, A new method for water suppression in the proton NMR spectra of aqueous solutions, J. Magn. Reson. 54 (1983) 539–542.
[10] V. Sklenar, A. Bax, Spin-Echo water suppression for the generation of pure-phase two-dimensional NMR-spectra, J. Magn. Reson. 74 (1987) 469–479.
[11] P. Hore, Solvent suppression in Fourier transform nuclear magnetic resonance, J. Magn. Reson. 55 (1983) 283–300.
[12] D. Turner, Binomial solvent suppression. J. Magn. Reson. 54 (1983) 146–148.
[13] M. Bak, J.T. Rasmussen, N.C. Nielsen, SIMPSON: a general simulation program for solid-state NMR spectroscopy, J. Magn. Reson. 147 (2000) 296–330. Available at: <www.bionmr.chem.au.dk>.
[14] Z. Tošner, T. Vosegaard, C. Kehlet, N. Khaneja, S.J. Glaser, N.C. Nielsen, Optimal control in NMR spectroscopy: numerical implementation in SIMPSON, J. Magn. Reson. 197 (2009) 120–134. Available at: <www.bionmr.chem.au.dk>.
[15] D.G. Norris, C. Schwarzbauer, Velocity selective radiofrequency pulse trains, J. Magn. Reson. 137 (1999) 231–236.
[16] Mathematica Edition: Version 7.0, Wolfram Research, Inc., Champaign, Illinois, 2008.
[17] P.M. Joseph, R.M. Summers, The flip-angle effect: a method for detection of sodium-23 quadrupole splitting in tissue, Magn. Reson. Med. 4 (1987) 67–77.
[18] S. Romanzetti, M. Halse, J. Kaffanke, K. Zilles, B. Balcom, N. Shah, A comparison of three SPRITE techniques for the quantitative 3D imaging of the 23Na spin density on a 4 T whole-body machine, J. Magn. Reson. 179 (2006) 64–72.
[19] M.D. Abramoff, P.J. Magelhaes, S.J. Ram, Image processing with image, J. Biophoton. Int. 11 (2004) 36–42.